Dynamic Scheduling in NR-V2X Mode 2: Probability of Successful Packet Delivery and Packet Inter-Reception

Luca Lusvarghi[1], Maria Luisa Merani[2,3], *Senior Member, IEEE*
Federico Pasquinucci[2,3] and Mattia Andreani[2,3]
[1]UWICORE Laboratory, Universidad Miguel Hernandez de Elche (UMH), 03202 Elche, Spain
[2]University of Modena and Reggio Emilia, 41125 Modena, Italy
[3]Consorzio Nazionale Interuniversitario per le Telecomunicazioni (CNIT), 43124 Parma, Italy
e-mail: llusvarghi@umh.es, {marialuisa.merani, federico.pasquinucci, mattia.andreani}@unimore.it .

***Abstract*—This work provides the first set of analytical tools to evaluate the performance of the dynamic scheduling scheme introduced in the 5G New Radio Vehicle-to-Everything standard to support direct vehicle-to-vehicle communications. It determines the probability of correctly receiving a packet as a function of the distance between the transmitting and the receiving vehicle, and statistically characterizes the time lag between the successful reception of two consecutive packets belonging to the same service flow. The analysis encompasses all the causes of packet losses, ranging from transmission impairments due to the hostile vehicular communication environment, to collisions and half-duplex radio limitations. Rigorous simulations validate the approach, demonstrating its accuracy and disclosing the influence of several parameters on system performance.**

***Index Terms*—NR-V2X, V2V, Mode 2, Dynamic Scheduling Scheme, Vehicular Networks, Analytical Models, Packet Delivery Ratio, Packet Inter-Reception**

I. Introduction

In the Cooperative, Connected, and Automated Mobility (CCAM) vision, Vehicle-to-Everything (V2X) connectivity plays a crucial role, as it allows Connected Vehicles (CVs) to extend their field of view beyond the Line-Of-Sight (LOS) range of the on-board sensors and of the human driver. Through V2X, CVs will be able coordinate their driving maneuvers by exchanging information about their position and dynamics, the detected objects, and the planned trajectories [1].

As of today, two V2X technologies have been considered by regulatory bodies for supporting the transition towards CCAM, namely IEEE 802.11p and Cellular V2X (C-V2X) [2]. On the one hand, IEEE 802.11p and its evolution, IEEE 802.11bd, are considered mature technologies after several years of simulative, analytical, and experimental investigations. On the other hand, C-V2X is a more recent technology standardized by 3GPP in 2017, under the LTE umbrella, and recently upgraded to 5G. Both the LTE and the 5G version of the C-V2X technology, respectively known as LTE-V2X and New Radio V2X (NR-V2X), feature a unique Sidelink (SL) interface that allows CVs to directly communicate without the need to relay the exchanged data through the cellular infrastructure [3]. Vehicle-to-Vehicle (V2V) SL communications are critical to provide seamless vehicular connectivity and guarantee CCAM in out-of-coverage contexts where the support of the cellular infrastructure is not available.

At Medium Access Control (MAC) sublayer, SL communications rely on two distributed resource allocation modes, known as LTE-V2X Mode 4 and NR-V2X Mode 2, that allow CVs to select transmission resources autonomously. Namely, NR-V2X Mode 2 has been introduced to complement its LTE-V2X Mode 4 predecessor with novel features and functionalities designed to guarantee a more effective and flexible assignment and management of resources. To this end, NR-V2X Mode 2 includes a new re-evaluation mechanism, a preemption mechanism, and features two alternative scheduling mechanisms known as Semi-Persistent Scheduling (SPS) and Dynamic Scheduling (DS).

NR-V2X Mode 2 has recently attracted plenty of attention in the V2X community. Over the last few years, several research papers relied on system-level simulations to assess its performance and explore the potential of Mode 2 for serving CCAM applications expected to generate periodic and aperiodic traffic with variable latency and reliability requirements. To this aim, the authors of [4] presented a detailed analysis of the NR-V2X Mode 2 re-evaluation mechanism, examining a complete set of system configurations and traffic types. In [5], the same authors provided a comparative analysis of the SPS and DS schemes considering variable latency requirements; they demonstrated that the DS scheme outperforms the SPS solution when CVs generate aperiodic traffic, a condition very often encountered in actual vehicular environments, as shown in [6]. The authors of [7] analyzed the impact of different physical (PHY) layer and MAC sublayer choices on the communication range and scheduling accuracy of the SPS scheme. One additional relevant contribution that relied on system-level simulations to investigate the NR-V2X Mode 2 performance was provided in [8], where the impact of blind re-

The work of F. Pasquinucci was partly supported by a Ferrari S.p.A. grant. This work was partially supported by the European Union under the Italian National Recovery and Resilience Plan (NRRP) of NextGenerationEU, partnership on "Telecommunications of the Future" (PE00000001 - program "RESTART").

transmissions on the performance of the SPS and DS schemes was analyzed.

Due to the high cost of NR-V2X prototypes and the practical limitations of real-world large-scale experimental studies, system-level simulations represent an appropriate and effective tool for the assessment of the NR-V2X Mode 2 performance. However, to accurately replicate the complex and intertwined functionalities of the NR-V2X protocol stack, existing simulators exhibit a significant complexity. Even when relying on dedicated hardware, e.g., simulation clusters, system-level simulations can require a long time, especially when the number of CVs and/or the amount of exchanged packets is large.

Conversely, analytical models represent a compact evaluation instrument to capture the NR-V2X Mode 2 behavior under a wide range of parameters and conditions. The analytical methodology typically relies on simplifying assumptions to make the mathematical derivation tractable; yet, if the model can identify and incorporate the most meaningful system features, it successfully characterizes the system behavior with negligible execution times and excellent accuracy.

As of today, modeling efforts in the NR-V2X community have exclusively focused on the SPS scheme, setting aside the analytical investigation of the DS solution. This is where the main contribution of the present work lies. In this paper, a novel set of analytical tools is proposed, to assess the DS scheme performance in a realistic vehicular setting - namely, a highway environment - assuming that CVs generate aperiodic traffic. This assumption realistically reflects the nature of the traffic generated by V2X-enabled CCAM applications, as demonstrated by the experimental studies in [6] and [9], and is also aligned with the insights offered by the studies in [5] and [8], where it is numerically demonstrated that the DS scheme should only be employed to accommodate aperiodic traffic. The analysis focuses on the two Key Performance Indicators (KPIs) included in the 3GPP evaluation guidelines [10], i.e., the Packet Delivery Ratio (PDR) and the Packet Inter-Reception (PIR). The former is defined as the ratio between the successfully received packets over the total number of transmitted packets and is provided as a function of the distance between the transmitting and the receiving vehicle. The latter is defined as the time between two consecutive successful receptions of packets belonging to the same application flow, and is a critical KPI for CCAM services that require a regular information exchange.

The proposed set of analytical tools offers an *a priori* estimate of the PDR, analytically determining the probability of successful packet delivery, P_{succ}. In addition, it provides the complete statistical characterization of the PIR, deriving its mean and Probability Density Function (PDF) in closed-form. The accuracy of the proposed analytical approach is validated against system-level simulation results obtained for various choices of system parameters. Numerical results confirm the DS scheme performance insights anticipated by the PDR and PIR analytical characterization: (i) P_{succ} is insensitive to the latency requirements of data traffic; (ii) when subject to increasingly high loads of aperiodic traffic, the DS scheme is unable to guarantee high values of P_{succ} and tightly confine the PIR values, even at relatively modest transmitter-receiver distances.

The remainder of the paper is organized as follows: Section II provides a survey of the scientific contributions dealing with the C-V2X performance evaluation. Section III outlines the most significant NR-V2X SL elements and describes the Mode 2 resource allocation mode. Section IV details the modeling assumptions that underpin this work. Section V illustrates the analytical derivations of the probability of successful packet delivery and Section VI provides the closed-form expression of the PIR mean value and PDF. Section VII proves the excellent accuracy of the proposed analysis through extensive system-level simulations and Section VIII concludes the paper.

II. Related Work

Analytical models are a powerful investigation instrument to characterize the performance of complex systems. For this reason, the V2X community devoted considerable research efforts to the modeling of C-V2X SL communications since their inception, in 2017. The first analytical model dates back to 2018, when the authors of [11] estimated the probability of successful packet delivery that characterizes the SPS solution in LTE-V2X Mode 4. Stemming from [11], an abundant body of literature focused on the SPS modeling. However, as the survey reported in this Section demonstrates, all existing works concentrate on the SPS scheme and no research efforts were devoted to the analytical characterization of the DS scheme. Regarding LTE-V2X Mode 4, the authors of [12] proposed a novel mathematical representation of the SPS operation and analyzed the impact of the channel load on the PDR. The contribution in [13] relied on Moment Matching Approximation (MMA) to obtain the statistics of the Signal-to-Interference-plus-Noise Ratio (SINR) and presented an SPS analytical model tailored to the platooning use case. Similarly, the authors of [14] put forth a mathematical approach to evaluate the performance of cooperative perception applications and again, focused upon SPS. When considering NR-V2X Mode 2, the study in [15] developed a probabilistic model of the SPS scheduling mechanism and critically analyzed its performance, highlighting the sensing limitations due to the half-duplex transceivers.

A further research line on C-V2X SL communications was characterized by the adoption of Markov chain-based approaches. Illustrative contributions in this category are [16] - [19]. In [16], a multi-dimensional Discrete Time Markov Chain (DTMC) was put forth to portray the MAC layer performance of LTE-V2X Mode 4 and 802.11p. This work was extended by the same authors in [17], examining multiple parallel data streams with different priority levels. Unlike the present study, both papers encompassed no modeling of the physical layer. In [18], Markov chains were employed to verify the SPS ability to fulfill the reliability and latency requirements of vehicle platooning. Here too, little consideration was paid to the modeling of the SL communication channel. A more recent contribution in this domain was [19], where Brady et al. developed a model to evaluate the PDR and the throughput attained by the SPS scheme in NR-V2X Mode 2, introducing some channel effects.

TABLE I
MAIN CONTRIBUTIONS TO THE ANALYTICAL MODELING OF C-V2X SL COMMUNICATIONS

	Mode 4	Mode 2		Channel effects	Model	Simulation
		SPS	DS			
M. Gonzalez-Martín *et. al.*, "Analytical Models of the Performance of C-V2X Mode 4 Vehicular Communications" [11]	✓	✗	✗	✓	✓	✓
F. Zhang *et al.*, "Mathematical Representation for Reliability of Sensing-Based Semi-Persistent Scheduling in LTE-V2X" [12]	✓	✗	✗	✗	✓	✓
A. Rehman *et al.*, "Analytical Modeling of Multiple Access Interference in C-V2X Sidelink Communications" [13]	✓	✗	✗	✓	✓	✓
F. A. Schiegg *et al.*, "Analytical Performance Evaluation of the Collective Perception Service in C-V2X Mode 4 Networks" [14]	✓	✗	✗	✗	✓	✗
A. Bazzi *et al.*, "On Wireless Blind Spots in the C-V2X Sidelink" [15]	✗	✓	✗	✓	✓	✓
G. P. Wijesiri *et al.*, "A Discrete-Time Markov Chain Based Comparison of the MAC Layer Performance of C-V2X Mode 4 and IEEE 802.11p" [16]	✓	✗	✗	✗	✓	✗
G. P. Wijesiri *et al.*, "The Effect of Concurrent Multi-Priority Data Streams on the MAC Layer Performance of IEEE 802.11p and C-V2X Mode 4" [17]	✓	✗	✗	✗	✓	✓
X. Giu. *et al.*, "Markov Analysis of C-V2X Resource Reservation for Vehicle Platooning" [18]	✓	✗	✗	✓	✓	✓
C. Brady *et al.*, "Modeling of NR C-V2X Mode 2 Throughput" [19]	✗	✓	✗	✓	✓	✓
A. Bazzi *et al.*, "On the Performance of IEEE 802.11p and LTE-V2V for the Cooperative Awareness of Connected Vehicles" [20]	✓	✗	✗	✗	✓	✓
A. Rolich *et al.*, "Impact of Persistence on the Age of Information in 5G NR-V2X Sidelink Communications" [21]	✗	✓	✗	✗	✓	✓
L. Cao *et al.*, "Optimize Semi-Persistent Scheduling in NR-V2X: An Age-of-Information Perspective" [22]	✗	✓	✗	✗	✓	✓

Meaningful contributions were also offered in estimating the performance of the two competing technologies, IEEE 802.11p and C-V2X. The results of [16] and [17] evidenced that, in the case of periodic traffic, LTE-V2X Mode 4 guarantees lower collision probability levels than its IEEE counterpart. Bazzi et al. also performed a comparative study based on analytical models in [20]. In this work, the authors compared the two radio access technologies when disseminating periodic Cooperative Awareness Messages (CAMs) and showed that LTE-V2X Mode 4 attains higher reliability levels than IEEE 802.11p as the transmitter-receiver distance increases. All of the above studies assumed periodic traffic patterns, an assumption abandoned by the present investigation.

On the other hand, the freshness of information is quite an unexplored research theme in the C-V2X domain. In [21], the authors developed an analytical model of the SPS scheme in NR-V2X Mode 2 to evaluate the average Age of Information (AoI) and Peak AoI (PAoI), assuming ideal communications between vehicles. In parallel, the study in [22] analyzed the NR-V2X Mode 2 SPS parameters from an AoI perspective, to assess the freshness guaranteed to small-size and periodic safety messages. The current work differs from the previous contributions in several ways. First, it focuses on the PIR, a standard-compliant metric similar to the AoI that captures the time between consecutive updates. Secondly, it provides the complete statistical characterization of the PIR, determining its mean and PDF in closed form.

Table I visually summarizes the main analytical studies in the field of C-V2X SL communications, highlighting the main assumptions that underpin each work as well as the availability of a simulation-based approach to validate the analytical results.

It is manifest that the previous works scrutinized the SPS scheme and primarily the transmission of periodic safety messages: no research efforts were dedicated to analytically characterize the DS scheme behavior. The current paper fills the research gap, proposing a novel approach to *a priori* evaluate the PDR and the PIR attained by the DS solution when subject to aperiodic traffic. To the authors' knowledge, this is the first study to offer such contributions.

III. OVERVIEW OF NR-V2X SL

This Section introduces the main PHY and MAC layer features of the NR-V2X SL technology, with an emphasis on those elements that play a role in the proposed model. A complete NR-V2X SL description is provided in [23].

At PHY layer, NR-V2X SL employs a Cyclic Prefix (CP) - Orthogonal Frequency Division Multiplexing (OFDM) waveform that supports a flexible Subcarrier Spacing (SCS) configuration. The supported SCS values are given by $2^{\mu} \cdot 15$ kHz, where μ is the OFDM numerology index, $\mu = 0, 1, 2$. CVs share a portion of a contiguous frequency band which is pre-configured for SL transmissions and called Bandwidth Part (BWP) in the standard's language. The BWP can be as wide as 100 MHz and is organized in smaller units called Resource Blocks (RBs). Each RB consists of 12 OFDM subcarriers and spans for 180, 360, or 720 kHz, depending on the adopted OFDM numerology. CVs on the same BWP must be pre-configured with the same SCS. In the time domain, the radio frame is the reference unit. Each frame lasts 10 ms and is

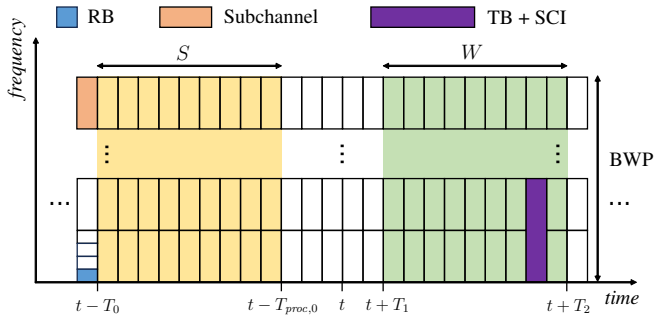

Fig. 1. Main PHY and MAC layer elements of the NR-V2X SL technology.

divided into ten 1 ms-long subframes. Based on the adopted numerology, every subframe includes a variable number of time slots. The number of time slots in a single subframe is 2^{μ} and the time slot duration is $t_s = 2^{-\mu}$ ms.

In NR-V2X SL, each packet is encapsulated in a data unit called Transport Block (TB). The TB is paired by the corresponding Sidelink Control Information (SCI), which carries fundamental information for the correct decoding of the TB such as the occupied RBs and the Modulation and Coding Scheme (MCS) employed for its transmission. The TB and the associated SCI are multiplexed on adjacent frequency resources and transmitted during the same time slot. Depending on the TB size and the MCS, the TB plus SCI transmission can occupy one or more subchannels. A subchannel is a group of contiguous RBs in the same time slot and represents the fundamental unit for packet transmission and reception. Fig. 1 portrays the above elements for the reference case where the subchannel is made of four RBs and the transmission of the TB and the SCI requires two subchannels.

At MAC sublayer, NR-V2X SL features two distinct resource allocation modes, termed Mode 1 and Mode 2. NR-V2X Mode 1 relies on the central orchestration of the cellular infrastructure to coordinate the assignment of the time-frequency transmission resources to CVs under network coverage. On the other hand, NR-V2X Mode 2 is a distributed resource allocation mode that does not require the support of the cellular infrastructure and, therefore, can be employed by CVs also in out-of-coverage conditions. In NR-V2X Mode 2, CVs autonomously select the transmission resources employing two alternative scheduling solutions, termed SPS and DS. CVs adopting the SPS scheme select - and periodically reserve - resources for the transmission of several consecutive TBs. Information about the reserved resources is included in the SCI and its correct reception is key to the functioning of NR-V2X Mode 2. On the other hand, CVs employing the DS scheme select new resources for the transmission of each TB and do not reserve any resources. In both the SPS and DS schemes, the selection of new resources is ruled by two time-frequency windows, the selection window (W) and the sensing window (S) portrayed in Fig. 1. The operation of the SPS and DS schemes can be summarized as follows: given the packet is ready for transmission at the time slot beginning at t, the CV selects an adequate number of subchannels to fit the TB plus SCI transmission among the candidate resources included in W,

$$W = [t + T_1, t + T_2], \quad T_{2,min} \leq T_2 \leq \text{PDB}, \tag{1}$$

where T_1 is the processing time required by the CV to identify candidate resources, $T_{2,min}$ depends on the SCS and the TB priority, and PDB is the Packet Delay Budget. The width of the selection window defines the maximum latency that the generated packet can tolerate. The selection is random and takes place after removing from W those resources that have already been reserved by neighboring CVs. The identification of already reserved resources relies on the inspection of the SCIs received by neighboring CVs during the preceding sensing window S,

$$S = [t - T_0, t - T_{proc,0}], \tag{2}$$

where T_0 can be set to either 1100 ms or 100 ms, and $T_{proc,0}$ is the time required to complete the sensing procedure. The MAC sublayer parameters that identify the duration of the selection (W) and sensing window (S) are visually summarized in Fig. 1.

A novel feature of NR-V2X Mode 2 when compared to its LTE-V2X Mode 4 predecessor is the re-evaluation mechanism. The re-evaluation mechanism forces CVs to keep monitoring the status of the selected resources before transmitting a TB and the associated SCI. As in Mode 4, it is worth highlighting that retransmissions are not mandatory in Mode 2.

In summary, the primary distinction between the SPS and DS schemes lies in how radio resources for the transmission of new TBs are reserved. The DS scheme does not allow CVs to reserve any resources for their transmission. This means that each TB requires the selection of new subchannels within the selection window. In contrast, the SPS scheme allows CVs to periodically reserve resources for the transmission of new TBs, making the sensing window essential for identifying candidate resources. It is important to note that, when all CVs adopt the DS scheme and do not perform any retransmissions, there is no benefit from listening to prior transmissions in the sensing window. Equivalently stated, the sensing window serves no purpose for the DS scheme under these hypotheses.

TABLE II
MAIN ELEMENTS OF THE NR-V2X SL TECHNOLOGY

Name	Acronym/Symbol
Subcarrier Spacing	SCS
Bandwidth Part	BWP
Resource Block	RB
Time slot	none
Time slot duration	t_s
Subchannel	none
Transport Block	TB
Sidelink Control Information	SCI
Modulation and Coding Scheme	MCS
Semi-Persistent Scheduling	SPS
Dynamic Scheduling	DS
Sensing window	S
Selection window	W

Table II summarizes the main NR-V2X SL elements and the corresponding acronyms and symbols that this Section introduced.

IV. Modeling Assumptions

The present study concentrates on the DS scheme employed by CVs to autonomously select transmission resources. It follows that the generic CV randomly selects resources in W to transmit the generated TB and does not perform any resource reservations. No constraint is set on the transmission type, which can be unicast, groupcast, or broadcast, but retransmissions are not considered. The re-evaluation mechanism is not modeled, as [4] demonstrated that it has no impact on the DS scheme performance when a single transmission per TB is performed.

We denote the total number of subchannels in the BWP by N_f and the total number of time slots in W by N_t. Note that the pool of candidate resources in W consists of $N_f \times N_t$ subchannels. With no substantial loss of accuracy, we further assume that the end of the sensing window and the beginning of the selection window coincide, i.e., $T_{proc,0} = T_1 = 0$, so that the duration of W coincides with T_2.

The examined scenario consists of a straight road, as in the case of a sufficiently long highway segment. Similarly to existing works [20][24], the road is mapped to a real line, vehicles move at a constant speed and are assimilated to points. Moreover, the number of CVs on the road segment is modeled by a Poisson Point Process (PPP), whose rate coincides with the average vehicular density λ_v vehicles/km. As a result, the number N_v of CVs on a highway segment whose length is d km, d being fixed, is expressed by a Poisson distribution:

$$P[N_v = m] = \frac{(\lambda_v d)^m}{m!} \cdot e^{-\lambda_v d}, \quad m \geq 0. \tag{3}$$

As regards data traffic, every CV behaves as an independent and aperiodic traffic source that generates constant-size packets (or TBs). The number of subchannels required for the transmission of the generated TBs and the associated SCIs is denoted by R_f. In this work, we assume that the generated TBs are always transmitted over a single subchannel, i.e., $R_f = 1$.

Adhering to the traffic models reported in the 3GPP evaluation guidelines [10], the inter-generation time between consecutive packets, denoted by X, is a shifted exponential Random Variable (RV) with parameters λ_p and c. Accordingly, the PDF of X is defined as

$$f_X(x) = \begin{cases} \lambda_p \cdot e^{-\lambda_p (x-c)} & \text{if } x \geq c \\ 0 & \text{otherwise} \end{cases} \tag{4}$$

and its mean value is

$$E[X] = c + \frac{1}{\lambda_p}. \tag{5}$$

For each CV, the packet inter-generation times are assumed to be independent and identically distributed (IID) RVs.

From (4), note that the minimum packet inter-generation time is c. It follows that the condition $T_2 \leq c$ must hold to guarantee that packets are transmitted in the same order as they were generated and that no buffering at the transmitter is required. These are established requirements for the traffic generated by safety-critical V2X-enabled applications.

We are interested in evaluating the probability p that the CV generates at least one packet in a time slot of t_s ms. To determine p, we denote the inter-generation time between packet $j-1$ and packet j by X_j and introduce the RV Λ_h, defined as

$$\Lambda_h = \sum_{j=1}^{h} X_j \,. \tag{6}$$

Observe that Λ_h is a sum of h IID RVs, each obeying the shifted exponential PDF given in (4). The above RV is more conveniently re-written as

$$\Lambda_h = h \cdot c + \sum_{j=1}^{h} X'_j \tag{7}$$

where X'_j's are IID exponential RVs with mean $\frac{1}{\lambda_p}$. Next, we observe that the sum of the X'_j's corresponds to an Erlang RV of order h, wherefrom the Cumulative Distribution Function (CDF) of Λ_h is readily obtained:

$$F_{\Lambda_h}(x) = \begin{cases} 1 - \sum_{j=0}^{h-1} e^{-\lambda_p (x-hc)} \frac{(\lambda_p (x-hc))^j}{j!} & \text{if } x \geq h \cdot c \\ 0 & \text{otherwise} \end{cases} \tag{8}$$

Next, we evaluate $P[N_p(\tau) = h]$, the probability that $N_p(\tau)$, the number of packets the CV generates in the interval $(0, \tau)$, is equal to h. To this aim, we observe that

$$P[N_p(\tau) \geq h] = \sum_{i=h}^{\infty} P[N_p(\tau) = i] =$$

$$= P[N_p(\tau) = h] + \sum_{i=h+1}^{\infty} P[N_p(\tau) = i] \,, \tag{9}$$

and similarly

$$P[N_p(\tau) \geq h+1] = \sum_{i=h+1}^{\infty} P[N_p(\tau) = i] \,, \tag{10}$$

wherefrom it readily stems that $P[N_p(\tau) = h]$ can be expressed as

$$P[N_p(\tau) = h] = P[N_p(\tau) \geq h] - P[N_p(\tau) \geq h+1] \,. \tag{11}$$

As the following equality holds

$$P[N_p(\tau) \geq h] = P[\Lambda_h \leq \tau] \,, \tag{12}$$

i.e.,

$$P[N_p(\tau) \geq h] = F_{\Lambda_h}(\tau) \,, \tag{13}$$

the equation in (11) becomes

$$P[N_p(\tau) = h] = F_{\Lambda_h}(\tau) - F_{\Lambda_{h+1}}(\tau) \tag{14}$$

and, taking advantage of (8), it is rewritten as

$$P[N_p(\tau) = h] = \begin{cases} e^{-\lambda_p (\tau - hc)} \frac{(\lambda_p (\tau - hc))^h}{h!} & \text{if } \tau \geq h \cdot c \\ 0 & \text{otherwise} \end{cases} \tag{15}$$

TABLE III
GLOSSARY OF THE EMPLOYED MATHEMATICAL NOTATION

Symbol	Definition
N_f	Total number of subchannels
R_f	Number of required subchannels (TB+SCI)
N_t	Number of time slots in W
λ_p	Average packet generation rate [packets/s]
c	Minimum packet inter-generation time
X	Inter-generation time between consecutive packets
p	Probability that the CV generates a packet in t_s ms
λ_v	Average vehicular density [veh/km]
N_v	Number of CVs in d km

Finally, making use of (15) specialized to $h = 0$ and $\tau = t_s$, p is obtained as

$$p = 1 - P[N_p = 0 \text{ in a time slot}] = 1 - P[N_p(t_s) = 0] = 1 - e^{-\lambda_p t_s} . \quad (16)$$

It is interesting to observe that in all cases of practical interest, the condition $c > t_s$ is verified, as the minimum packet inter-generation is much larger than the time slot duration. This is demonstrated by the experimental studies reported in [6], [9] and captured by the analytical models defined by 3GPP in [10]. As a result, we conclude that, during a time slot, each CV either generates exactly one packet or none, that is,

$$p = P[N_p(t_s) = 1] . \quad (17)$$

We emphasize that p will be instrumental when determining the probability of successful packet delivery in the next Section. The most relevant symbols introduced above are reported in Table III.

V. Successful Packet Delivery

The aim of the current Section is to analytically determine the probability of successful packet delivery for a pair of transmitting and receiving CVs, termed v_t and v_r, respectively, which travel on the linear road populated by CVs in accordance with the previous hypotheses.

With no loss of generality, it is assumed that v_r is located at the origin of the distance axis, v_t is at a distance $d_{t,r}$ from v_r, and the interference due to CVs located outside the $[-D_{max}, +D_{max}]$ interval centered on v_r is negligible. As discussed in Section VII, the last assumption is readily verified by selecting a sufficiently large value of D_{max}.

Observe that a packet transmitted by v_t is successfully received by v_r only if the two mutually independent conditions reported below hold:

(i) v_r is not in transmission mode during the time slot in which v_t is engaged in the packet transmission. This constraint is due to the half-duplex limitations of NR-V2X radios;

(ii) the packet from v_t does not collide with packets transmitted by other vehicles and is successfully decoded despite the presence of noise and propagation impairments. Alternatively, the packet incurs in a collision, but despite the presence of noise, propagation impairments, and co-channel interference, it is successfully decoded.

Next, denote by

- P_{HD} the half-duplex probability, i.e., the probability that v_r is simultaneously transmitting on the same time slot as v_t and, therefore, cannot decode the transmitted packet;
- $P[N_v = m]$ the probability that m CVs are present in the $[-D_{max}, +D_{max}]$ interval centered on v_r;
- $P[n \text{ interfering transmissions} | N_v = m]$ the probability that $n \geq 0$ interfering packet transmissions spoil the correct packet delivery, conditioned on the presence of $N_v = m$ CVs in the $[-D_{max}, +D_{max}]$ interval;
- P_{SNR} the probability that the packet from v_t is not successfully decoded by v_r due to an insufficient Signal-to-Noise Ratio (SNR);
- P_{SINR_n} the probability that the packet from v_t is not successfully decoded by v_r due to an insufficient Signal-to-Interference-plus-Noise Ratio (SINR) in the presence of n interfering packet transmissions, $n > 0$.

It follows that P_{succ}, the probability of successful packet delivery when the distance between v_t and v_r is $d_{t,r}$, is expressed as:

$$P_{succ}(d_{t,r}) = P[\text{packet from } v_t \text{ successfully received by } v_r] = (1 - P_{HD}) \cdot \left\{ \sum_{m=0}^{\infty} \sum_{n=0}^{m} (1 - P_{SINR_n}(d_{t,r})) \times P[n \text{ interfering transmissions} | N_v = m] \cdot P[N_v = m] \right\} \quad (18)$$

where $P_{SINR_0} = P_{SNR}$ for the purpose of compact notation. Note that the independence between the previous conditions (i) and (ii) reflects in (18), where there appears the product of their occurrence probabilities, given by $(1 - P_{HD})$ and the double summation in the curly brackets, respectively.

The individual contributions in (18) are analytically derived in the remainder of this Section, in Subsection V-A through V-E.

A. The Half-Duplex Probability, P_{HD}

Let us start by examining the limit case where the selection window W consists of a single time slot, i.e., $N_t = 1$. Provided v_t has generated a packet and is ready for its transmission, the probability P_{HD} that v_r and v_t are simultaneously transmitting on the same time slot coincides with the probability that v_r generates a packet during the same time slot as v_t, that is,

$$P_{HD} = p , \quad (19)$$

p being provided by (16). Note that P_{HD} does not depend on R_f, the number of subchannels required for the TB plus SCI transmission.

When the number of time slots in W is greater than one, i.e., $N_t > 1$, CVs randomly and uniformly select the resources in W. This is the case since the DS scheme does not allow CVs to reserve any resources when retransmissions are not employed and, as a result, all subchannels included in W are considered available. Assuming that v_t transmits the generated TB on a generic time slot that begins at time t, observe that the same time slot is included in the selection window of v_r

for any packet that v_r generates in the preceding N_t slots. As the selection of resources is random in W, the probability of v_r selecting the same time slot as v_t is $\frac{1}{N_t}$ and, hence, the probability that v_r transmits on the same slot as v_t is

$$P_{HD} = p \cdot N_t \cdot \frac{1}{N_t} = p\,, \quad N_t > 1\,. \tag{20}$$

It is therefore concluded that P_{HD} is not affected by N_t, the number of time slots in W. As the time slot duration t_s is a constant for a given numerology index, this is equivalent to concluding that P_{HD} does not depend on the duration of the selection window W, i.e., on the packet latency limit T_2.

B. The Probability $P[N_v = m]$

The probability of having m CVs on a road segment that corresponds to the $[-D_{max}, +D_{max}]$ interval and, hence, is $2D_{max}$ km long, is immediately obtained from (3) by replacing d with $2D_{max}$

$$P[N_v = m] = \frac{(\lambda_v 2D_{max})^m}{m!} \cdot e^{-\lambda_v 2D_{max}}\,, \quad m \geq 0\,. \tag{21}$$

C. The Probability of n Interfering Packets

Let us next focus on the probability of having n interfering transmissions, i.e., n interfering packets, superimposed to the packet transmitted by v_t given that m CVs are present on the $[-D_{max}, +D_{max}]$ road segment centered on v_r.

Recalling that: (i) CVs generate packets independently; (ii) the probability that a CV generates one packet during a time slot is p; (iii) the selection of the transmission resources is random in W; (iv) every CV requires one subchannel, i.e., $R_f = 1$, then

$$P[n \text{ interfering transmissions} | N_v = m] = \binom{m}{n} \cdot \left(\frac{p}{N_f}\right)^n \cdot \left(1 - \frac{p}{N_f}\right)^{m-n}\,. \tag{22}$$

Note that the above expression corresponds to the probability that n out of m CVs generate one packet and transmit it on the same subchannel selected by v_t.

Like the half-duplex probability P_{HD}, the probability of having n interfering packet transmissions does not depend on N_t, i.e., the number of time slots in W, and is therefore independent of the latency requirements that the packets exhibit.

D. The Probability P_{SNR}

Next, the probability P_{SNR} that the packet from v_t cannot be successfully decoded by v_r due to an insufficient SNR is determined. To this aim, the characterization of the V2V propagation channel plays a fundamental role. Adhering to the 3GPP evaluation guidelines [10], the V2V propagation channel is modeled taking into account the path loss, shadowing, and multipath fading. Two channel states are considered, a LOS and a Non-Line-Of-Sight (NLOSv) state: in the former, a direct LOS path between v_t and v_r exists; in the latter, the direct LOS path between v_t and v_r is obstructed by the presence of other CVs. The LOS and NLOSv state occurrence probabilities are P_{LOS} and P_{NLOSv}, respectively, and their expressions are provided in Appendix A.

In both states, the path loss (PL) in dB is a function of the distance between the transmitting and the receiving vehicle, $d_{t,r}$, and the center frequency (in GHz) f_c:

$$PL(d_{t,r}) = c_1 + c_2 \cdot 10\log_{10}(d_{t,r}) + c_3 \cdot 10\log_{10}(f_c)\,. \tag{23}$$

where c_1, c_2, and c_3 are constants and are defined in [10].

In the LOS state, the received SNR (expressed in dB) due to the path loss and shadowing is

$$SNR_{LOS} = P_t - PL(d_{t,r}) + \mathcal{N}(0, \sigma) - N_0\,, \tag{24}$$

where P_t is v_t's transmission power in dB, $PL(d_{t,r})$ is given by (23), $\mathcal{N}(0, \sigma)$ is the zero-mean Gaussian RV with standard deviation σ that accounts for the shadowing, and N_0 is the noise power in dB. Thus, the SNR_{LOS} is a Gaussian RV itself, i.e.,

$$SNR_{LOS} = \mathcal{N}(\mu_{LOS}, \sigma_{LOS})\,, \tag{25}$$

its PDF being

$$f_{SNR_{LOS}}(s) = \frac{1}{\sqrt{2\pi}\sigma_{LOS}} e^{-\frac{(s-\mu_{LOS})^2}{2\sigma_{LOS}^2}}\,. \tag{26}$$

where

$$\mu_{LOS} = P_t - PL(d_{t,r}) - N_0 \tag{27}$$

and

$$\sigma_{LOS}^2 = \sigma^2\,. \tag{28}$$

In the NLOSv state, an additional Gaussian-distributed blockage loss with mean μ_{block} and standard deviation σ_{block} is introduced [10]. It follows that the received SNR, denoted by SNR_{NLOSv}, is a Gaussian RV,

$$SNR_{NLOSv} = \mathcal{N}(\mu_{NLOSv}, \sigma_{NLOSv}) \tag{29}$$

with mean

$$\mu_{NLOSv} = P_t - PL(d_{t,r}) - N_0 - \mu_{block}\,, \tag{30}$$

and variance

$$\sigma_{NLOSv}^2 = \sigma^2 + \sigma_{block}^2\,. \tag{31}$$

We denote its PDF by $f_{SNR_{NLOSv}}(x)$.

In the LOS and NLOSv states, multipath fading is rendered through a Clustered Delay Line (CDL) model [10]. As the complexity of the channel model prohibits the adoption of a closed form to capture the impact of fast fading on the correct packet delivery, we rely upon a numerical approach to provide the Packet Error Rate (PER) as a function of the SNR in the form of a Look Up Table (LUT). Note that the LUT is a widely accepted tool when a simple fast fading characterization is abandoned [11]. For a given CDL channel model, MCS, and Doppler shift, the LUT is obtained through extensive link-level simulations. We formally express the PER as follows

$$\text{PER}(SNR) = \begin{cases} 1, & \text{if } SNR \leq SNR_{thres} \\ f_{LUT}(SNR), & \text{otherwise} \end{cases}\,, \tag{32}$$

where SNR_{thres} is the minimum SNR required for triggering the packet decoding process at the receiver and $f_{LUT}(\cdot)$ is the function representing the LUT. Then, unconditioning the

PER with respect to the channel state and the SNR due to the path loss and shadowing, the probability P_{SNR} that the packet from v_t cannot be successfully decoded by v_r owing to an insufficient SNR is determined as follows:

$$P_{SNR}(d_{t,r}) = \left[\sum_{s=-\infty}^{+\infty} \mathrm{PER}(s) \cdot f_{SNR_{LOS}}(s)\right] \cdot P_{LOS} + \left[\sum_{s=-\infty}^{+\infty} \mathrm{PER}(s) \cdot f_{SNR_{NLOSv}}(s)\right] \cdot P_{NLOSv}\,. \quad (33)$$

In (33), note that the dependence on $d_{t,r}$ stems from (27) and (30), as well as from the state occurrence probabilities; this is revealed by the P_{LOS} and P_{NLOSv} expressions, provided in Appendix A, where the μ_{block} and σ^2_{block} expressions are also given.

E. The Probability P_{SINR_n}, $n > 0$

To determine P_{SINR_n}, it is assumed that the V2V channel between the i-th interfering vehicle v_i and v_r obeys the same statistical description as the channel between v_t and v_r and that all channels fade independently. The co-channel interference is postulated to play the predominant role; therefore, the Signal-to-Interference (SIR) ratio replaces the SINR and the probability of unsuccessful packet delivery in the presence of n interfering vehicles is denoted by P_{SIR_n}. The reasoning proceeds along the same lines as for the evaluation of P_{SNR}, except for the P_{SIR_n} dependence on the distances $d_{i,r}$, $i = 1, 2, \ldots, n$, between the interfering CVs and the receiving vehicle v_r.

When the v_t-v_r pair is in the LOS state, we denote by $SIR_{LOS,n}$ the SIR experienced at the receiver in the presence of path loss, shadowing, and co-channel interference generated by n interfering CVs:

$$SIR_{LOS,n} = P_t - PL(d_{t,r}) + \mathcal{N}(0,\sigma) - \mathcal{I}_n(\mathbf{\Delta}_n)\,. \quad (34)$$

where the term $\mathcal{I}_n$ accounts for the co-channel interference power in dB and depends on $\mathbf{\Delta}_n = \{d_{1,r}, \ldots, d_{n,r}\}$, the array of interferer-receiver distances. To highlight the $SIR_{LOS,n}$ dependence on $\mathbf{\Delta}_n$, we denote its PDF by $f_{SIR_{LOS,n}|\mathbf{\Delta}_n}(x)$.

Analogously, we indicate the SIR in the NLOSv state by $SIR_{NLOSv,n}$ and its PDF by $f_{SIR_{NLOSv,n}|\mathbf{\Delta}_n}(x)$.

We assimilate the interference power to noise and recalling (32), we write P_{SIR_n} as

$$P_{SIR_n}(d_{t,r}, \mathbf{\Delta}_n) = \left[\sum_{s=-\infty}^{+\infty} \mathrm{PER}(s) \cdot f_{SIR_{LOS,n}|\mathbf{\Delta}_n}(s)\right] \cdot P_{LOS} + \left[\sum_{s=-\infty}^{+\infty} \mathrm{PER}(s) \cdot f_{SIR_{NLOSv,n}|\mathbf{\Delta}_n}(s)\right] \cdot P_{NLOSv}\,. \quad (35)$$

To remove the $P_{SIR_n}(d_{t,r}, \mathbf{\Delta}_n)$ dependence on the interferer-receiver distances, (35) has to be unconditioned with respect to all possible locations of the n interfering CVs. To this end, observe that the PPP assumption on the number of vehicles introduced in Section IV implies that the distances $d_{i,r}$, $i = 1, 2, \ldots, n$, are uniformly distributed RVs in $[-D_{max}, +D_{max}]$.

Hence, once we introduce the unconditional PDF of the $SIR_{LOS,n}$, $f_{SIR_{LOS,n}}$,

$$f_{SIR_{LOS,n}}(s) = \frac{1}{(2D_{max})^n} \int \cdots \int_{\mathcal{D}} f_{SIR_{LOS,n}|\mathbf{\Delta}_n}(s)\, d\mathbf{\Delta}_n\,, \quad (36)$$

where the integration domain is

$$\mathcal{D} = \begin{cases} -D_{max} \le d_{1,r} \le +D_{max} \\ -D_{max} \le d_{2,r} \le +D_{max} \\ \ldots \\ -D_{max} \le d_{n,r} \le +D_{max} \end{cases} \quad (37)$$

and, similarly, the unconditional PDF of the $SIR_{NLOSv,n}$, denoted by $f_{SIR_{NLOSv,n}}$,

$$f_{SIR_{NLOSv,n}}(s) = \frac{1}{(2D_{max})^n} \int \cdots \int_{\mathcal{D}} f_{SIR_{NLOSv,n}|\mathbf{\Delta}_n}(s)\, d\mathbf{\Delta}_n\,, \quad (38)$$

then we can write P_{SIR_n}, the probability of unsuccessful packet delivery in the presence of n interfering transmissions, as

$$P_{SIR_n}(d_{t,r}) = \left[\sum_{s=-\infty}^{+\infty} \mathrm{PER}(s) \cdot f_{SIR_{LOS,n}}(s)\right] \cdot P_{LOS} + \left[\sum_{s=-\infty}^{+\infty} \mathrm{PER}(s) \cdot f_{SIR_{NLOSv,n}}(s)\right] \cdot P_{NLOSv}\,. \quad (39)$$

Although there is no closed form expression for $f_{SIR_{LOS,n}}(s)$ in (36) and $f_{SIR_{NLOSv,n}}(s)$ in (38), an accurate analytical fitting of these PDFs can be provided. Under the modeling assumptions on $SIR_{LOS,n}$ and $SIR_{LOSv,n}$, the log-gamma PDF is an appropriate choice. It follows that $f_{SIR_{LOS,n}}(s)$ is given by

$$f_{SIR_{LOS,n}}(s) \simeq \frac{e^{\beta_L(s-\eta_L)} e^{-e^{(s-\eta_L)/\alpha_L}}}{\alpha_L^{\beta_L}\Gamma(\beta_L)}\,, \quad \Gamma(\beta_L) = (\beta_L - 1)! \quad (40)$$

α_L being the scale parameter, β_L the shape parameter, and η_L the location parameter. Similarly, $f_{SIR_{NLOSv,n}}(s)$ is approximated by a log-gamma PDF whose parameters are denoted by α_N, β_N and η_N. Appendix B reports the proposed analytical expressions of the scale, shape, and location parameters. Furthermore, Section VII will provide evidence of the fitting accuracy.

Once $f_{SIR_{LOS,n}}(s)$ and $f_{SIR_{NLOSv,n}}(s)$ expressions are replaced in (39), the probability of unsuccessful packet delivery P_{SIR_n} in the presence of $n > 0$ interfering CVs is obtained.

At this point, all the terms appearing in (18) are dissected and the path to determine P_{succ}, the probability of successful packet delivery, is set. In this regard, recall that the half-duplex probability in (20) and the probability of n interfering packet transmissions in (22) do not depend on T_2, the duration of the selection window. Further, note that T_2 plays no role in the P_{SNR} and P_{SIR_n} evaluation too. Hence, we can conclude that P_{succ} does not depend on T_2, i.e., on the latency requirements that the generated packets exhibit.

VI. Packet Inter-Reception

In this Section, the analytical determination of the PIR PDF is provided. For a given pair of transmitting and receiving vehicles, the PIR is the time between two consecutive successful receptions of packets belonging to the same application flow. The PIR is a particularly relevant KPI for applications that are sensitive to the time between updates, e.g., platooning, and it is a metric included in the 3GPP evaluation guidelines for V2X [10].

To derive the PIR PDF, we interpret the selection window W as a temporal continuum, as opposed to a finite sequence of time slots. Hence, the DS random selection of a time slot for the packet transmission translates into the choice of a time sample in $[t, t+T_2]$ following a uniform distribution.

Let us begin by considering PIR_0, the PIR conditioned on no packet losses, and let t_{rx_0} and t_{rx_1} denote the reception times of the two consecutive and successfully received packets. By definition PIR_0 is

$$\text{PIR}_0 = t_{rx_1} - t_{rx_0}\,. \tag{41}$$

Neglecting the propagation delay and the packet transmission time t_s, which is an acceptable hypothesis for single hop, short-range communications, (41) is equivalently formulated as

$$\text{PIR}_0 = t_{tx_1} - t_{tx_0}\,, \tag{42}$$

where t_{tx_0} and t_{tx_1}, $t_{tx_0} < t_{tx_1}$, are the transmission times of the two packets received at time t_{rx_0} and t_{rx_1}, respectively. They are illustrated in Fig. 2(a) and expressed as follows:

$$\begin{aligned} t_{tx_0} &= t_{gen_0} + U_0 \\ t_{tx_1} &= t_{gen_1} + U_1\,, \end{aligned} \tag{43}$$

where t_{gen_0} and t_{gen_1} are the generation times of the two packets, and U_0 and U_1 are two independent and uniformly distributed RVs in the $[0, T_2]$ interval. Replacing (43) in (42), PIR_0 is rewritten as

$$\begin{aligned} \text{PIR}_0 &= t_{gen_1} + U_1 - (t_{gen_0} + U_0) \\ &= t_{gen_1} - t_{gen_0} + U_1 - U_0 = X_1 + U_1 - U_0, \end{aligned} \tag{44}$$

where $X_1 = t_{gen_1} - t_{gen_0}$ denotes the inter-generation time between the two packets. From Section IV, we recall that X_1 is an RV that follows the shifted exponential PDF provided in (4).

Next, consider PIR_1, the PIR conditioned on a single packet loss. As shown in Fig. 2(b), let t_{tx_0} and t_{tx_2} denote the transmission instants of the two successfully received packets, and let t_{tx_1} denote the transmission instant of the incorrectly received packet, $t_{tx_0} < t_{tx_1} < t_{tx_2}$. In this circumstance, PIR_1 is expressed as

$$\begin{aligned} \text{PIR}_1 = t_{rx_2} - t_{rx_0} = t_{tx_2} - t_{tx_0} &= t_{gen_2} + U_2 - (t_{gen_0} + U_0) \\ &= t_{gen_2} - t_{gen_0} + U_2 - U_0\,, \end{aligned} \tag{45}$$

where in analogy to the previously introduced notation, U_2 is a uniform RV in $[0, T_2]$. Denoting by X_2 the inter-generation

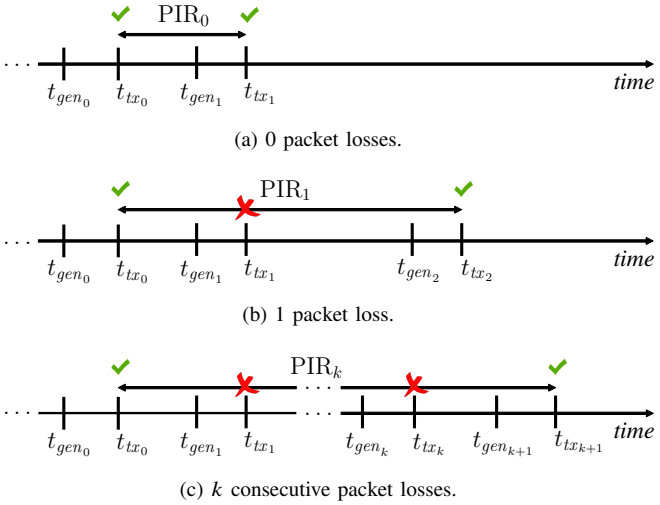

Fig. 2. PIR illustration conditioned on 0, 1, and k consecutive packet losses.

time between the second and the third packet of the sequence, it is immediate to conclude that PIR_1 can be re-written as

$$\begin{aligned} \text{PIR}_1 &= (t_{gen_2} - t_{gen_1}) + (t_{gen_1} - t_{gen_0}) + U_2 - U_0 \\ &= X_2 + X_1 + U_2 - U_0\,, \end{aligned} \tag{46}$$

Through a proper iteration of the reasoning that led to (44) and (46), PIR_k, the PIR conditioned on the occurrence of k consecutive packet losses (illustrated in Fig. 2(c)) is written as

$$\text{PIR}_k = t_{rx_{k+1}} - t_{rx_0} = t_{tx_{k+1}} - t_{tx_0} = \sum_{j=1}^{k+1} X_j + U_{k+1} - U_0\,. \tag{47}$$

where X_j is the inter-generation time between the $(j-1)$-th and the j-th packet and U_{k+1} a uniform RV in $[0, T_2]$.

Recalling from Section IV that the X_j's are IID RVs and observing that U is a uniformly distributed RV in $[0, T_2]$, the average PIR, $E[\text{PIR}]$, is obtained from (47) unconditioning with respect to k,

$$E[\text{PIR}] = (E[K] + 1) \cdot E[X] \tag{48}$$

in which $E[K]$ denotes the mean of the RV K, K representing the number of consecutive packet losses. If we assume that packets are independently affected by losses, $E[K]$ results

$$\begin{aligned} E[K] &= \sum_{k=0}^{+\infty} k \cdot P[K = k] \\ &= \sum_{k=0}^{+\infty} k \cdot (1 - P_{succ}(d_{t,r}))^k P_{succ}(d_{t,r}) = \frac{1 - P_{succ}(d_{t,r})}{P_{succ}(d_{t,r})}\,, \end{aligned} \tag{49}$$

and taking advantage of $E[X]$ expression in (5), $E[\text{PIR}]$ is finally obtained as

$$E[\text{PIR}] = \frac{1}{P_{succ}(d_{t,r})} \cdot \left(c + \frac{1}{\lambda_p}\right)\,. \tag{50}$$

It is therefore concluded that $E[\text{PIR}]$ is a function of the distance $d_{t,r}$ between v_t and v_r and is inversely proportional to the probability of correctly receiving a packet; as such, its minimum value coincides with the mean inter-generation

$$f_{\mathrm{PIR}_k}(x) = \begin{cases} 0 & \text{if } x < (k+1)c - T_2 \\ -\frac{1}{k!\lambda_p T_2^2} \cdot \Big[(k+1)! + k!\lambda_p \left((k+1)c - T_2 - x \right) & \\ \qquad + (-1)^{k+1} e^{\lambda_p ((k+1)c - T_2 - x)} \Psi^{(1,k+1)}(x + T_2) \Big] & \text{if } (k+1)c - T_2 < x < (k+1)c \\ \frac{1}{k!\lambda_p T_2^2} \cdot \Big[(k+1)! + k!\lambda_p \left((k+1)c + T_2 - x \right) + (-1)^{k+1} 2 e^{\lambda_p ((k+1)c - x)} \Psi^{(1,k+1)}(x) & \\ \qquad + (-1)^{k} e^{\lambda ((k+1)c - T_2 - x)} \Psi^{(1,k+1)}(x + T_2) \Big] & \text{if } (k+1)c < x < (k+1)c + T_2 \\ \frac{(-1)^k e^{\lambda_p ((k+1)c - T_2 - x)}}{k!\lambda_p T_2^2} \cdot \Big[\Psi^{(1,k+1)}(x + T_2) - 2 e^{\lambda_p T_2} \Psi^{(1,k+1)}(x) & \\ \qquad + e^{2\lambda_p T_2} \Psi^{(1,k+1)}(x - T_2) \Big] & \text{if } x > (k+1)c + T_2 \end{cases} \tag{57}$$

$$\Psi^{(i,k)}(x) = \begin{cases} 1 & \text{if } i = k \\ \frac{(-1)^{k-i} (k-1)! (k-i+1)}{(i-1)!} + \lambda_p \left(kc - x \right) \Psi^{(i+1,k)}(x) & \text{otherwise} \end{cases} \tag{58}$$

time, whereas its maximum is not upper-bounded. Moreover, as P_{succ} is a decreasing function of $d_{t,r}$, $E[\mathrm{PIR}]$ increases for higher distances between v_t and v_r.

We next proceed with the determination of the PIR PDF. In accordance with the symbology introduced in Section IV, in (47) we denote by Λ_{k+1} the RV

$$\Lambda_{k+1} = \sum_{j=1}^{k+1} X_j \,. \tag{51}$$

The PDF of Λ_{k+1} can be obtained as the derivative of (8), where h has been replaced by $k+1$, leading to

$$f_{\Lambda_{k+1}}(x) = \\ = \begin{cases} \frac{-\lambda_p^{k+1} \left((k+1)c - x \right)^k e^{\lambda_p ((k+1)c - x)}}{k!} & \text{if } x \geq (k+1) \cdot c \\ 0 & \text{otherwise} \end{cases} \tag{52}$$

Once we further introduce the RV S_{k+1}, defined as

$$S_{k+1} = U_{k+1} - U_0 \,, \tag{53}$$

the PIR_k is formulated as

$$\mathrm{PIR}_k = \Lambda_{k+1} + S_{k+1} \,. \tag{54}$$

As regards the RV S_{k+1} in (53), it represents the difference between two IID uniform RVs in $[0, T_2]$; it therefore obeys the triangular PDF given below

$$f_{S_{k+1}}(x) = \begin{cases} \frac{x}{T_2^2} + \frac{1}{T_2} & \text{if } -T_2 \leq x \leq 0 \\ -\frac{x}{T_2^2} + \frac{1}{T_2} & \text{if } 0 \leq x \leq T_2 \\ 0 & \text{otherwise} \end{cases} \,. \tag{55}$$

Hence, the PDF of PIR_k conditioned on k is given by the convolution of the PDFs in (52) and (55),

$$f_{\mathrm{PIR}_k}(x) = \int_{-\infty}^{+\infty} f_{\Lambda_{k+1}}(z) f_{S_{k+1}}(x - z) dz \,, \quad -\infty < x < \infty \,. \tag{56}$$

In Appendix C, it is demonstrated that the closed-form solution of the above integral is provided by (57), where there appears the function $\Psi^{(i,k)}(x)$ detailed in (58), which evidences the PIR dependence on T_2, the duration of the selection window.

Once $f_{\mathrm{PIR}_k}(x)$ is known, the last step to statistically characterize the PIR consists in unconditioning $f_{\mathrm{PIR}_k}(x)$ with respect to K, i.e.,

$$f_{\mathrm{PIR}}(x) = \sum_{k=0}^{+\infty} f_{\mathrm{PIR}_k}(x) \cdot P_{succ}(d_{t,r}) \cdot (1 - P_{succ}(d_{t,r}))^k \,. \tag{59}$$

Note that $f_{\mathrm{PIR}}(x)$ depends on P_{succ}, hence, on the distance $d_{t,r}$ between the transmitting and the receiving vehicles. The accuracy of (59) will be numerically demonstrated in the next Section for different choices of system parameters.

VII. Numerical Results

A. Examined Scenario

We validate the analysis of the probability of successful packet delivery and of the packet inter-reception in a simulated environment that consists of a 5 km long highway segment with six lanes, three per driving direction. The width of each lane is 4 m. CVs on the slowest lane travel at 70 km/h, on the intermediate lane at 90 km/h, and on the fastest lane at 110 km/h.

The main NR-V2X SL PHY layer parameters are reported in Table IV. The center frequency and channel bandwidth are equal to 5.9 GHz and 20 MHz, respectively [25]. Following the ETSI recommendations in [26], the examined OFDM numerology is set to $\mu = 1$, which implies that the SCS is

TABLE IV
MAIN NR-V2X SL PHY LAYER PARAMETERS

Parameter	Value
Center frequency, f_c	5.9 GHz
Channel bandwidth	20 MHz
SCS	30 kHz
Number of subcarriers	12
RB bandwidth	$30 \cdot 12 = 360$ kHz
Modulation type	16 QAM
TB code rate	0.49
SCI code rate	0.08
Total number of subchannels	$N_f = 4$
Transmission power, P_t	23 dBm
Shadowing std. deviation, σ	3 dB
Receiver sensitivity level	-103.5 dBm
Thermal noise PSD	-174 dBm/Hz
Noise figure	9 dBm

30 KHz, the time slot duration $t_s = 0.5$ ms, and the RB bandwidth 360 kHz. Each subchannel is made of 12 RBs [26], which results in 4 available subchannels in the considered 20 MHz bandwidth. The CVs transmit packets whose size is 200 bytes; note that 200 bytes is the smallest statistically relevant packet size value reported in the experimental study on CAM statistics published at [9]. The selected MCS is 13, which mandates for 16-QAM modulation, a TB code rate equal to 0.49, and an SCI code rate equal to 0.08 [27]; this implies that the TB plus SCI transmission requires one out of the four available subchannels, i.e., $R_f = 1$. Moreover, the SNR_{thres} is equal to -4.86 dBm, derived from the assumptions that the receiver sensitivity level is -103.5 dBm [28], the noise figure is 9 dB [10], and the thermal noise power spectral density is the Johnson-Nyquist noise level, equal to 174 dBm/Hz.

The D_{max} value is set equal to 1374 m and corresponds to the distance at which the average signal power due to the path loss and the shadowing coincides with the noise power. It was numerically verified that larger D_{max} values lead to negligible variations in all the numerical evaluations.

To avoid border effects, all metrics are computed considering the central 2 kilometers of the highway.

B. Model Validation

First, the accuracy of the log-gamma approximation for $f_{SIR_{LOS,n}}$ and $f_{SIR_{NLOSv,n}}$ is verified. For every value of n, we derive the PDFs by Monte Carlo simulation and then obtain their analytical approximations, by properly tuning the log-gamma coefficients in (62), (63), and (64) of Appendix B. Such coefficients were numerically determined and are provided in Table V. As an illustrative example, Fig. 3(a) shows the comparison between the PDF reconstructed by simulation and the log-gamma PDF in the LOS state for $n = 5$, when different $d_{t,r}$ values ($d_{t,r} = 10$, 100 and 1000 m) are considered; the figure reveals that the fitting is more than satisfying. Next, Fig. 3(b) confirms the accuracy of the log-gamma approximation in the LOS case considering a varying number of interfering packet transmissions ($n = 5$, $n = 10$, and $n = 20$) and a fixed distance between v_t and v_r, namely

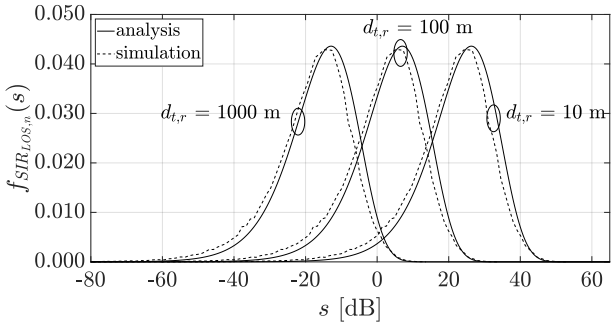

(a) $n = 5$.

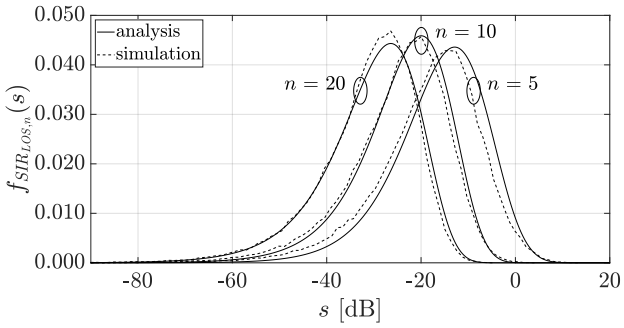

(b) $d_{t,r} = 1000$ m.

Fig. 3. Accuracy of the $f_{SIR_{LOS,n}}(s)$ log-gamma approximation for different values of $d_{t,r}$ and n.

$d_{t,r} = 1000$ m. Similar trends have also been obtained in the NLOSv case. Moreover, we *a posteriori* verified that it is the location parameter (η_L in the LOS state, η_N in the NLOSv state) to play the most significant role in the P_{succ} evaluation.

The focus now shifts to evaluating the probability of successful packet delivery. To this end, the LUT we adopted in (32) is the one provided in [29]. In the implementation of (18), we stop the summation in m when $m = 3 \cdot \lambda_v D_{max}$. This value corresponds to three times the standard deviation of the Poisson RV that models the number of CVs in the $[-D_{max}, +D_{max}]$ interval and covers the 99.7% of the distribution. To show the accuracy and effectiveness of the analysis, Figs. 4(a)-(c) report P_{succ} and the PDR obtained through simulations as a function of $d_{t,r}$. The simulation results are obtained through MoReV2X, a fully-fledged NR-V2X simulator, developed by some of the authors of this work [30]. Three different vehicular densities, namely, $\lambda_v = 50$, 100, and 200 vehicles/km, are examined, to reflect increasingly crowded road conditions. In Fig. 4(a), the minimum packet inter-generation time is $c = 50$ ms and $\lambda_p^{-1} = 50$ ms, leading to an average packet inter-generation time $E[X] = 100$ ms. In Fig. 4(b), $c = \lambda_p^{-1} = 20$ ms, hence $E[X] = 40$ ms and, lastly, in Fig. 4(c), $c = \lambda_p^{-1} = 10$ ms, so that $E[X] = 20$ ms.

The figures reveal that there is an almost perfect overlap between the analytical and simulated curves. The figures also quantitatively highlight the effects of an increasing vehicular density λ_v and a decreasing packet inter-generation time $E[X]$, which are both responsible for a growing number of collisions, hence for the deterioration of P_{succ}. Note that, when $E[X] = 20$ ms, Fig. 4(c) shows that the NR-V2X DS scheme falls short

TABLE V
FITTING COEFFICIENTS OF THE LOG-GAMMA PARAMETERS

Parameter	Coefficients						
α_L	$c_{1,L}^{(\alpha)} = 13.67$	$c_{2,L}^{(\alpha)} = 0.13$	$c_{3,L}^{(\alpha)} = 5.93$	$c_{4,L}^{(\alpha)} = 1.67$	$c_{5,L}^{(\alpha)} = 8.87$	-	-
β_L	$c_{1,L}^{(\beta)} = 6220$	$c_{2,L}^{(\beta)} = 0.06$	$c_{3,L}^{(\beta)} = 45.86$	$c_{4,L}^{(\beta)} = 0.46$	$c_{5,L}^{(\beta)} = 1.12$	-	-
η_L	$c_{1,L}^{(\eta)} = 2.58$	$c_{2,L}^{(\eta)} = 13.87$	$c_{3,L}^{(\eta)} = 26.09$	$c_{4,L}^{(\eta)} = 0$	$c_{5,L}^{(\eta)} = 0$	$c_{6,L}^{(\eta)} = 8.69$	$c_{7,L}^{(\eta)} = 55.63$
α_N	$c_{1,N}^{(\alpha)} = 1.41$	$c_{2,N}^{(\alpha)} = 0.16$	$c_{3,N}^{(\alpha)} = 0.20$	$c_{4,N}^{(\alpha)} = 298.1$	$c_{5,N}^{(\alpha)} = 12.91$	-	-
β_N	$c_{1,N}^{(\beta)} = 659.7$	$c_{2,N}^{(\beta)} = 0.08$	$c_{3,N}^{(\beta)} = 29.43$	$c_{4,N}^{(\beta)} = 0.48$	$c_{5,N}^{(\beta)} = 1.79$	-	-
η_N	$c_{1,N}^{(\eta)} = 3.28$	$c_{2,N}^{(\eta)} = 16.82$	$c_{3,N}^{(\eta)} = 27.16$	$c_{4,N}^{(\eta)} = 0.15$	$c_{5,N}^{(\eta)} = 1.42$	$c_{6,N}^{(\eta)} = 11.91$	$c_{7,N}^{(\eta)} = 39.18$

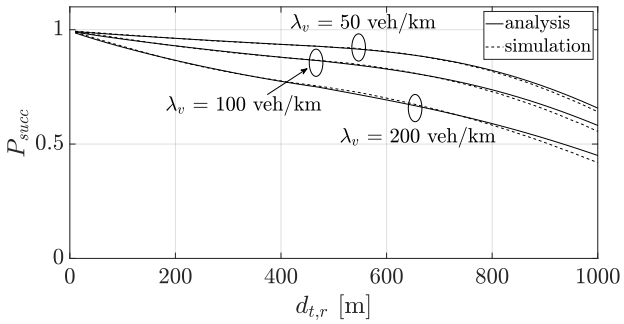

(a) $E[X]$ = 100 ms.

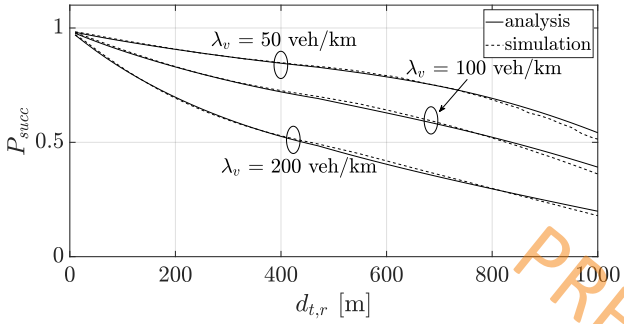

(b) $E[X]$ = 40 ms.

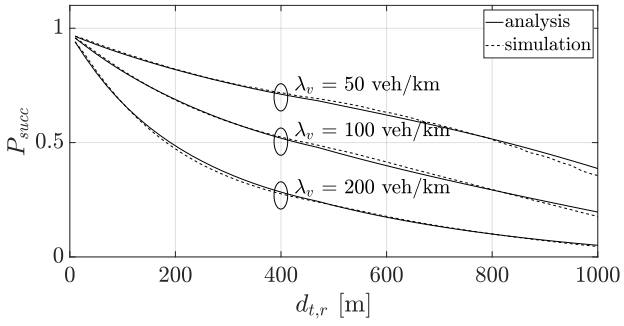

(c) $E[X]$ = 20 ms.

Fig. 4. P_{succ} as a function of $d_{t,r}$.

in guaranteeing P_{succ} values greater than 0.9, i.e., the minimum reliability requirement for V2X-enabled CCAM applications identified by 3GPP in [31], even at low $d_{t,r}$ values.

It is worth highlighting that the analytical approach guarantees a drastic saving in computational time when compared to simulation. We employed a computer equipped with 8 3 GHz Intel i7-9700 cores, 16 GB RAM, and a 512 GB solid state disc; the MoReV2X simulator ran on the Ubuntu distribution

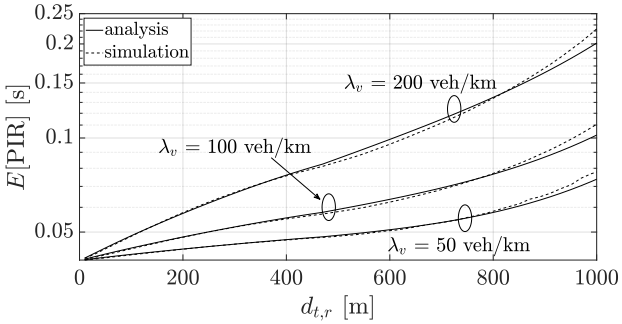

Fig. 5. E[PIR] as a function of $d_{t,r}$, $E[X]$ = 40 ms.

of Linux, version 20.04.6 LTS. For the lowest vehicular density and the highest average packet inter-generation time, i.e., λ_v = 200 veh/km and $E[X]$ = 100 ms, the single simulation run to obtain the P_{succ} curve (1000 points with a $d_{t,r}$ step equal to 20 m) required 3592 s to complete, approximately 24 hours. The heaviest simulation, referring to λ_v = 200 veh/km and $E[X]$ = 20 ms, required 389273 s, nearly four and a half days. Moreover, the simulations were repeated for 10 different seeds and their outcomes averaged, to warrant accurate P_{succ} estimates. The analysis led to the same results, but in a handful of seconds (approximately 4.2 seconds total run time), with a computational saving of several orders of magnitude.

Next, Fig. 5 shows E[PIR] as a function of $d_{t,r}$ for the same choice of parameters as in Fig. 4(b). The figure evidences that E[PIR] rises above 40 ms, the average inter-generation time, as soon as $d_{t,r}$ becomes greater than 10 m. Here too, the analysis provides results that are extremely close to the simulation outcomes.

Figs. 6(a)-(c) report the Complementary Cumulative Distribution Function (CCDF) of the PIR, obtained by numerical integration of the PDF given by (59), and the CCDF obtained by simulation. These figures refer to an illustrative distance between v_t and v_r equal to $d_{t,r}$ = 100 m, different values of the vehicular density, λ_v = 50, 100, and 200 veh/km, and T_2 = PDB, where PDB = c. The same values considered in Fig. 4(a)-(c) are examined, namely c = 10, 20, and 50 ms, and λ_p = 100, 50, and 20 packets/s, so that $E[X]$ = 20, 40, and 100 ms. These figures demonstrate that the analytical approach always provides an upper bound - and an accurate estimate - to the PIR CCDF. Moreover, the figures quantify the remarkable influence of T_2 on the PIR statistics, as predicted by (55) and (59). As an example, Fig. 6(c) shows that, for T_2 = PDB = 10 ms and λ_v = 200 vehicles/km, the probability

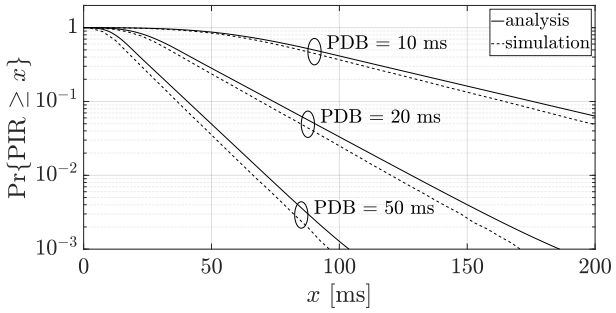

(a) λ_v = 50 veh/km.

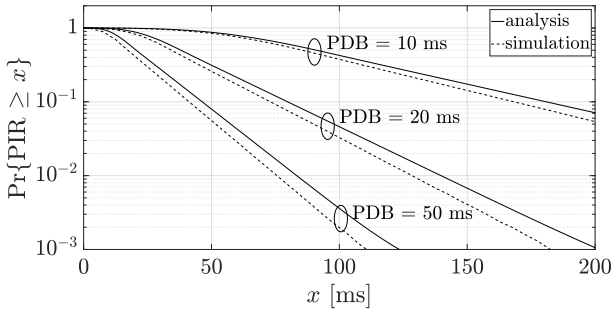

(b) λ_v = 100 veh/km.

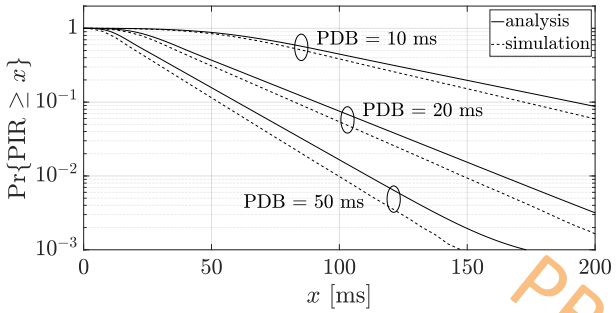

(c) λ_v = 200 veh/km.

Fig. 6. PIR CCDF for different λ_v values when $d_{t,r}$ = 100 m.

the packets incur into PIR values greater than 200 ms is close to 0.1, which is very likely to violate the delay requirements of real-time safety services.

VIII. Conclusions

This work has presented a novel set of analytical tools to assess the performance achieved by the NR-V2X Mode 2 DS scheme in a highway scenario. The proposed tools model the probability of successfully receiving a packet as a function of the distance between the transmitting and the receiving vehicle, and offer a complete statistical description of the PIR. The analysis takes into account all causes of packet losses, namely, the half-duplex radios, the access strategy the DS scheme implements, noise, co-channel interference due to packet collisions, and the transmission impairments due to the hostile V2V propagation environment. Additionally, it captures the effects of application characteristics and requirements, including the average packet generation rate and the maximum tolerated latency, on the performance of the DS scheme. Therefore, the analytical models proposed in this study serve as a valuable tool for preliminarily investigating the performance of V2V-enabled services, such as platooning and extended sensors, when supported by the DS scheme. The comparison between the analysis and the simulation outcomes has proved the accuracy of the proposed analytical approach. It has also numerically confirmed the insights provided by the analytical models on the influence of several parameters on the DS scheme performance; most notably, the P_{succ} insensitivity to the selection window duration, hence the PDB, and the remarkable influence this has on the PIR. The study has also shown that in the examined setting the DS scheme is unable to fulfill the stringent requirements set by advanced safety applications.

Appendix A

The V2V channel model adopted in this work adheres to the description in [10]. For V2V SL communications in the highway scenario, [10] indicates that the LOS state occurrence probability P_{LOS} is a function of the distance $d_{t,r}$ between the transmitting and the receiving vehicle, namely,

$$P_{LOS} = \begin{cases} \min[1, a \cdot d_{t,r}^2 + b \cdot d_{t,r} + c], & \text{if } d_{t,r} \leq d_{thres} \\ \max[0, a' - b' \cdot (d_{t,r} - d_{thres})], & \text{otherwise} \end{cases} \quad (60)$$

where d_{thres} = 475 m, $a = 2.1013 \cdot 10^{-6}$, $b = -0.002$, $c = 1.0193$, $a' = 0.54$, and $b' = 0.001$.

In the LOS and NLOSv states, the shadow fading is lognormally distributed with dB spread $\sigma = 3$. In the NLOSv state, we examined the intermediate case in which the blocker antenna height is between the minimum and the maximum of the antenna height of the transmitting and receiving CV. As indicated in [10], an additional blockage loss is therefore introduced, lognormally distributed, with mean in dB

$$\mu_{block} = 5 + \max\left[0, c_{1_{block}} \cdot \log_{10}(d_{t,r}) - c_{2_{block}}\right] \quad (61)$$

$c_{1_{block}}$ = 15 and $c_{2_{block}}$, and standard deviation σ_{block} = 4 dB.

As regards fast fading, the number of clusters and the number of rays per cluster in the channel impulse response, their delays, and angular spreads are those provided in [10] for the highway environment.

Appendix B

The parameters of the log-gamma PDF $f_{SIR_{LOS,n}}(\cdot)$ in (40) are approximated in closed form as follows:

$$\alpha_L(n) = c_{1,L}^{(\alpha)} \cdot \exp[-(c_{2,L}^{(\alpha)} \cdot (n + c_{3,L}^{(\alpha)}))^2] \cdot \ln(n + c_{4,L}^{(\alpha)}) + c_{5,L}^{(\alpha)} \quad (62)$$

$$\beta_L(n) = c_{1,L}^{(\beta)} \cdot \exp[-(c_{2,L}^{(\beta)} \cdot (n + c_{3,L}^{(\beta)}))^2] \cdot \ln(n + c_{4,L}^{(\beta)}) + c_{5,L}^{(\beta)} \quad (63)$$

$$\begin{aligned} \eta_L(n, d_{t,r}) = & - c_{1,L}^{(\eta)} \cdot \ln^3(n) + c_{2,L}^{(\eta)} \cdot \ln^2(n) \\ & - c_{3,L}^{(\eta)} \cdot \ln(n) - c_{4,L}^{(\eta)} \cdot \ln^3(d_{t,r}) \\ & + c_{5,L}^{(\eta)} \cdot \ln^2(d_{t,r}) - c_{6,L}^{(\eta)} \cdot \ln(d_{t,r}) + c_{7,L}^{(\eta)} \end{aligned} \quad (64)$$

The above expressions indicate that α_L and β_L exclusively depend on n, the number of interfering CVs, whereas η_L depends on n and $d_{t,r}$, the distance between v_t and v_r.

The parameters of the $f_{SIR_{NLOSv,n}}(s)$ function obey the same expressions with different coefficients, namely, $\alpha_N(n)$, $\beta_N(n)$, and $\eta_N(n, d_{t,r})$. All coefficients are reported in Table V.

APPENDIX C

As highlighted by (56), the PDF of PIR_k is the result of the convolution between the PDFs in (52) and (55). Given they are piecewise functions, the result of the convolution is a piecewise function too. To this end, it can be graphically demonstrated that there are four domains of x to be separately considered when solving the convolution, namely,

$$\begin{aligned}\mathcal{D}_0 &= (-\infty, (k+1)c - T_2] \\ \mathcal{D}_1 &= [(k+1)c - T_2, (k+1)c] \\ \mathcal{D}_2 &= [(k+1)c, (k+1)c + T_2] \\ \mathcal{D}_3 &= [(k+1)c + T_2, +\infty)\end{aligned} \tag{65}$$

Depending on the considered domain, the integrand functions and the integration region change, affecting the result of (56).

When $x \in \mathcal{D}_0$, the PIR_k PDF is

$$f_{\text{PIR}_k,\mathcal{D}_0}(x) = 0 \tag{66}$$

When $x \in \mathcal{D}_1$, the PIR_k PDF is

$$f_{\text{PIR}_k,\mathcal{D}_1}(x) = \int_{(k+1)c}^{x+T_2} \frac{-\lambda_p^{k+1}\left((k+1)c - z\right)^k e^{\lambda_p((k+1)c-z)}}{k!} \times \left(\frac{x-z}{T_2^2} + \frac{1}{T_2}\right) dz. \tag{67}$$

After a few lengthy steps, the above integral can be solved by partial integration, yielding the closed-form expressions reported in (68) for $k = 0, 1, 2, 3$. Although the derivation of $f_{\text{PIR}_k,\mathcal{D}_1}(x)$ is limited to $k = 3$ for the sake of readability, a careful inspection reveals a regular pattern in the obtained expressions. Employing the recursive function in (58), the PIR_k PDF can be generalized to an arbitrary number of k consecutive packet losses by induction, obtaining the expression reported in (57) for $x \in \mathcal{D}_1$.

When $x \in \mathcal{D}_2$, the PIR_k PDF is determined by solving the following integral through partial integration

$$\begin{aligned}&f_{\text{PIR}_k,\mathcal{D}_2}(x) = \\ &= \int_x^{x+T_2} \frac{-\lambda_p^{k+1}\left((k+1)c - z\right)^k e^{\lambda_p((k+1)c-z)}}{k!} \left(\frac{x-z}{T_2^2} + \frac{1}{T_2}\right) dz \\ &+ \int_{(k+1)c}^{x} \frac{-\lambda_p^{k+1}\left((k+1)c - z\right)^k e^{\lambda_p((k+1)c-z)}}{k!} \left(\frac{z-x}{T_2^2} + \frac{1}{T_2}\right) dz.\end{aligned} \tag{69}$$

The results obtained for $k = 0, 1, 2, 3$ are reported in (70) and, also in this case, by leveraging the recursive function in (58) it is possible to generalize the expression of f_{PIR_k} by induction and obtain the expression reported in (57) for $x \in \mathcal{D}_2$.

Last, when $x \in \mathcal{D}_3$, the integral in (56) specializes in

$$\begin{aligned}&f_{\text{PIR}_k,\mathcal{D}_3}(x) = \\ &= \int_x^{x+T_2} \frac{-\lambda_p^{k+1}\left((k+1)c - z\right)^k e^{\lambda_p((k+1)c-z)}}{k!} \left(\frac{x-z}{T_2^2} + \frac{1}{T_2}\right) dz \\ &+ \int_{x-T_2}^{x} \frac{-\lambda_p^{k+1}\left((k+1)c - z\right)^k e^{\lambda_p((k+1)c-z)}}{k!} \left(\frac{z-x}{T_2^2} + \frac{1}{T_2}\right) dz,\end{aligned} \tag{71}$$

and its closed-form solution is reported in (72) for $k = 0, 1, 2, 3$. Following the same inductive approach as before, the expression of the PIR_k PDF can be generalized for an arbitrary number of consecutive packet losses, obtaining the expression reported in (57) for $x \in \mathcal{D}_3$.

REFERENCES

[1] 5GAA, "C-V2X Use Cases: Methodology, Examples and Service Level Requirements," 5GAA White Paper, Jul. 2019.

[2] G. Naik, B. Choudhury and J. -M. Park, "IEEE 802.11bd & 5G NR V2X: Evolution of Radio Access Technologies for V2X Communications," in *IEEE Access*, vol. 7, pp. 70169-70184, May 2019.

[3] 3GPP, "Overall description of radio access network (RAN) aspects for vehicle-to-everything (V2X) based on LTE and NR (v16.1.0, release 16)," 3GPP, Sophia Antipolis, France, Rep. TR 37.985, Apr. 2022.

[4] A. Molina-Galan, L. Lusvarghi, B. Coll-Perales, J. Gozalvez and M. L. Merani, "On the Impact of Re-Evaluation in 5G NR V2X Mode 2," in *IEEE Trans. on Veh. Tech.*, vol. 73, no. 2, pp. 2669-2683, Feb. 2024.

[5] L. Lusvarghi *et al.*, "A Comparative Analysis of the Semi-Persistent and Dynamic Scheduling Schemes in NR-V2X Mode 2" in *Elsevier Vehicular Communications*, vol. 42, Jun. 2023.

[6] L. Lusvarghi, C. A. Grazia, M. Klapez, M. Casoni and M. L. Merani, "Awareness Messages by Vulnerable Road Users and Vehicles: Field Tests Via LTE-V2X," in *IEEE Transactions on Intelligent Vehicles*, vol. 8, no. 10, pp. 4418-4433, Oct. 2023.

[7] V. Todisco *et al.*, "Performance Analysis of Sidelink 5G-V2X Mode 2 Through an Open-Source Simulator," in *IEEE Access*, vol. 9, pp. 145648-145661, Oct. 2021.

[8] C. Campolo, V. Todisco, A. Molinaro, A. Berthet, S. Bartoletti and A. Bazzi, "Improving Resource Allocation for beyond 5G V2X Sidelink Connectivity," 2021 55th Asilomar Conference on Signals, Systems, and Computers, Pacific Grove, CA, USA, pp. 55-60, Oct. 2021.

[9] CAR 2 CAR Communication Consortium, "Survey on ITS-G5 CAM statistics," TR2052, V1.0.1, Dec. 2018.

[10] 3GPP, "Study on evaluation methodology of new Vehicle-to-Everything (V2X) use cases for LTE and NR," TR 37.885, Rel-15 V15.3.0, Jun. 2019.

[11] M. Gonzalez-Martín, M. Sepulcre, R. Molina-Masegosa and J. Gozalvez, "Analytical Models of the Performance of C-V2X Mode 4 Vehicular Communications," in *IEEE Trans. on Veh. Tech.*, vol. 68, no. 2, pp. 1155-1166, Feb. 2019.

[12] F. Zhang *et al.*, "Mathematical Representation for Reliability of Sensing-Based Semi-Persistent Scheduling in LTE-V2X," in *IEEE Trans. on Veh. Tech.*, vol. 71, no. 9, pp. 10115-10119, Sep. 2022.

[13] A. Rehman *et al.*, "Analytical Modeling of Multiple Access Interference in C-V2X Sidelink Communications," 2022 IEEE MeditCom, Athens, Greece, pp. 215-220, Sep. 2022.

[14] F. A. Schiegg, N. Brahmi and I. Llatser, "Analytical Performance Evaluation of the Collective Perception Service in C-V2X Mode 4 Networks," 2019 IEEE Intelligent Transportation Systems Conference (ITSC), Auckland, New Zealand, pp. 181-188, Oct. 2019.

[15] A. Bazzi *et al.*, "On Wireless Blind Spots in the C-V2X Sidelink," in *IEEE Trans. on Veh. Tech.*, vol. 69, no. 8, pp. 9239-9243, Aug. 2020.

[16] G. P. Wijesiri N.B.A., J. Haapola and T. Samarasinghe, "A Discrete-Time Markov Chain Based Comparison of the MAC Layer Performance of C-V2X Mode 4 and IEEE 802.11p," in *IEEE Transactions on Communications*, vol. 69, no. 4, pp. 2505-2517, Apr. 2021.

[17] G. P. Wijesiri N. B. A, J. Haapola and T. Samarasinghe, "The Effect of Concurrent Multi-Priority Data Streams on the MAC Layer Performance of IEEE 802.11p and C-V2X Mode 4," in *IEEE Transactions on Communications*, vol. 70, no. 1, pp. 592-605, Jan. 2022.

[18] X. Gu *et al.*, "Markov Analysis of C-V2X Resource Reservation for Vehicle Platooning," 2022 IEEE 95th Vehicular Technology Conference: (VTC2022-Spring), Helsinki, Finland, pp. 1-5, Jun. 2022.

[19] C. Brady, L. Cao and S. Roy, "Modeling of NR C-V2X Mode 2 Throughput," 2022 IEEE International Workshop Technical Committee on Communications Quality and Reliability (CQR), Arlington, VA, USA, pp. 19-24, Sep. 2022.

[20] A. Bazzi *et al.*, "On the Performance of IEEE 802.11p and LTE-V2V for the Cooperative Awareness of Connected Vehicles," in *IEEE Trans. on Veh. Tech.*, vol. 66, no. 11, pp. 10419-10432, Nov. 2017.

[21] A. Rolich, I. Turcanu, A. Vinel and A. Baiocchi, "Impact of Persistence on the Age of Information in 5G NR-V2X Sidelink Communications," 2023 21st MedComNet, Island of Ponza, Italy, pp. 15-24, Jun. 2023.

$$f_{\mathrm{PIR}_k,\mathcal{D}_1}(x)=\begin{cases}\frac{-1}{\lambda_p T_2^2}\left[1+\lambda_p(c-T_2-x)-e^{\lambda_p(c-T_2-x)}\right] & \text{if } k=0\\ \frac{-1}{\lambda_p T_2^2}\cdot\left[2+\lambda_p(2c-T_2-x)-e^{\lambda_p(2c-T_2-x)}[-2+\lambda_p(2c-T_2-x)]\right] & \text{if } k=1\\ \frac{-1}{2\lambda_p T_2^2}\cdot\left[6+\lambda_p(6c-2(T_2-x))-e^{\lambda_p(3c-T_2-x)}[6+\lambda_p(3c-T_2-x)(-4+\lambda_p(3c-T_2-x))]\right] & \text{if } k=2\\ \frac{-1}{6\lambda_p T_2^2}\cdot\left[24+\lambda_p(24c-6(T_2-x))\right. & \\ \quad\left.-e^{\lambda_p(4c-T_2-x)}[-24+\lambda_p(4c-T_2-x)(18+\lambda_p(4c-T_2-x)(-6+\lambda_p(4c-T_2-x)))]\right] & \text{if } k=3\end{cases} \tag{68}$$

$$f_{\mathrm{PIR}_k,\mathcal{D}_2}(x)=\begin{cases}\frac{1}{\lambda_p T_2^2}\cdot\left[1+\lambda_p(c+T_2-x)-2e^{\lambda_p(c-x)}+e^{\lambda_p(c-T_2-x)}\right] & \text{if } k=0\\ \frac{1}{\lambda_p T_2^2}\cdot\left[2+\lambda_p(2c+T_2-x)+2e^{\lambda_p(2c-x)}\left[-2+\lambda_p(2c-x)\right]-e^{\lambda_p(2c-T_2-x)}\left[-2+\lambda_p(2c-T_2-x)\right]\right] & \text{if } k=1\\ \frac{1}{2\lambda_p T_2^2}\cdot\left[6+2\lambda_p(3c+T_2-x)-2e^{\lambda_p(3c-x)}\left[6+\lambda_p(3c-x)(-4+\lambda_p(3c-x))\right]\right. & \\ \quad\left.+e^{\lambda_p(3c-T_2-x)}\left[6+\lambda_p(3c-T_2-x)(-4+\lambda_p(3c-T_2-x))\right]\right] & \text{if } k=2\\ \frac{1}{6\lambda_p T_2^2}\cdot\left[24+6\lambda_p(4c+T_2-x)+2e^{\lambda_p(4c-x)}\left[-24+\lambda_p(4c-x)(18+\lambda_p(4c-x)(-6+\lambda_p(4c-x)))\right]\right. & \\ \quad\left.-e^{\lambda_p(4c-T_2-x)}\left[-24+\lambda_p(4c-T_2-x)(18+\lambda_p(4c-T_2-x)(-6+\lambda_p(4c-T_2-x)))\right]\right] & \text{if } k=3\end{cases} \tag{70}$$

$$f_{\mathrm{PIR}_k,\mathcal{D}_3}(x)=\begin{cases}\frac{e^{\lambda_p(c-T_2-x)}}{\lambda_p T_2^2}\cdot\left[1-2e^{\lambda_p T_2}+e^{2\lambda_p T_2}\right] & \text{if } k=0\\ \frac{-e^{\lambda_p(2c-T_2-x)}}{\lambda_p T_2^2}\cdot\left[-2+\lambda_p(2c-T_2-x)-2e^{\lambda_p T_2}\left[-2+\lambda_p(2c-x)\right]+e^{2\lambda_p T_2}\left[-2+\lambda_p(2c+T_2-x)\right]\right] & \text{if } k=1\\ \frac{e^{\lambda_p(2c-T_2-x)}}{2\lambda_p T_2^2}\cdot\left[6+\lambda_p(3c-T_2-x)(-4+\lambda_p(3c-T_2-x))\right. & \\ \quad\left.-2e^{\lambda_p T_2}\left[6+\lambda_p(3c-x)(-4+\lambda_p(3c-x))\right]\right. & \\ \quad\left.+e^{2\lambda_p T_2}\left[6+\lambda_p(3c+T_2-x)(-4+\lambda_p(3c+T_2-x))\right]\right] & \text{if } k=2\\ \frac{-e^{\lambda_p(4c-T_2-x)}}{6\lambda_p T_2^2}\cdot\left[-24+\lambda_p(4c-T_2-x)(18+\lambda_p(4c-T_2-x)(-6+\lambda_p(4c-T_2-x)))\right. & \\ \quad\left.-2e^{\lambda_p T_2}\left[-24+\lambda_p(4c-x)(18+\lambda_p(4c-x)(-6+\lambda_p(4c-x)))\right]\right. & \\ \quad\left.+e^{2\lambda_p T_2}\left[-24+\lambda_p(4c+T_2-x)(18+\lambda_p(4c+T_2-x)(-6+\lambda_p(4c+T_2-x)))\right]\right] & \text{if } k=3\end{cases} \tag{72}$$

[22] L. Cao, H. Yin, R. Wei and L. Zhang, "Optimize Semi-Persistent Scheduling in NR-V2X: An Age-of-Information Perspective," 2022 IEEE WCNC, Austin, TX, USA, pp. 2053-2058, Apr. 2022.

[23] M. H. C. Garcia *et al.*, "A Tutorial on 5G NR V2X Communications," in IEEE Communications Surveys & Tutorials, vol. 23, no. 3, pp. 1972-2026, Feb. 2021.

[24] M. I. Hassan, H. L. Vu and T. Sakurai, "Performance Analysis of the IEEE 802.11 MAC Protocol for DSRC Safety Applications," in *IEEE Trans. on Veh. Tech.*, vol. 60, no. 8, pp. 3882-3896, Oct. 2011.

[25] 5G Automotive Associations (5GAA), "Deployment band configuration for C-V2X at 5.9 GHz in Europe," 5GAA Position Paper, Jun. 2021.

[26] ETSI, "Intelligent Transport Systems (ITS); LTE-V2X and NR-V2X Access layer specification for Intelligent Transport Systems operating in the 5 GHz frequency band; Release 2," EN 303 798 V1.1.7, Jun. 2021.

[27] ETSI, "5G; NR; Physical layer procedures for data (3GPP TS 38.214 version 16.4.0 Release 16),", TS 138 214 V16.4.0, Jan. 2021.

[28] 5GAA, "V2X Functional and Performance Test Report; Test Procedures and Results," 5GAA Test Report, Apr. 2019.

[29] 3GPP, "Link level evaluations of NR PSSCH," R1-1903181, 3GPP TSG-RAN WG1 Meeting 96, Mar. 2019. [Online]. Available: https://www.3gpp.org/ftp/TSG_RAN/WG1-RL1/TSGR1-96/Docs/R1-1903181.zip

[30] L. Lusvarghi and M. L. Merani, "MoReV2X - A New Radio Vehicular Communication Module for ns-3," 2021 IEEE 94th Vehicular Technology Conference (VTC2021-Fall), Virtual event, pp. 1-7, Sep. 2021.

[31] 3GPP, "TS 22.186 5G; Service requirements for enhanced V2X scenarios (v16.2.0, Release 16)," 3GPP, Tech. Spec., Nov. 2020.